JACS
JOURNAL OF THE AMERICAN CHEMICAL SOCIETY
Article
pubs.acs.org/JACS

Hot-Electron-Induced Highly Efficient O_2 Activation by Pt Nanoparticles Supported on Ta_2O_5 Driven by Visible Light

Hirokatsu Sakamoto,[†] Tomoyuki Ohara,[†] Naoki Yasumoto,[†] Yasuhiro Shiraishi,*[,†,‡] Satoshi Ichikawa,[∥] Shunsuke Tanaka,[§] and Takayuki Hirai[†]

[†]Research Center for Solar Energy Chemistry, and Division of Chemical Engineering, Graduate School of Engineering Science, Osaka University, Toyonaka 560-8531, Japan

[‡]PRESTO, JST, Saitama 332-0012, Japan

[∥]Institute for NanoScience Design, Osaka University, Toyonaka 560-8531, Japan

[§]Department of Chemical, Energy and Environmental Engineering, Kansai University, Suita 564-8680, Japan

Supporting Information

ABSTRACT: Aerobic oxidation on a heterogeneous catalyst driven by visible light (λ >400 nm) at ambient temperature is a very important reaction for green organic synthesis. A metal particles/semiconductor system, driven by charge separation via an injection of "hot electrons (e_{hot}^-)" from photoactivated metal particles to semiconductor, is one of the promising systems. These systems, however, suffer from low quantum yields for the reaction (<5% at 550 nm) because the Schottky barrier created at the metal/semiconductor interface suppresses the e_{hot}^- injection. Some metal particle systems promote aerobic oxidation via a non-e_{hot}^--injection mechanism, but require high reaction temperatures (>373 K). Here we report that Pt nanoparticles (~5 nm diameter), when supported on semiconductor Ta_2O_5, promote the reaction without e_{hot}^- injection at room temperature with significantly high quantum yields (~25%). Strong Pt−Ta_2O_5 interaction increases the electron density of the Pt particles and enhances interband transition of Pt electrons by absorbing visible light. A large number of photogenerated e_{hot}^- directly activate O_2 on the Pt surface and produce active oxygen species, thus promoting highly efficient aerobic oxidation at room temperature.

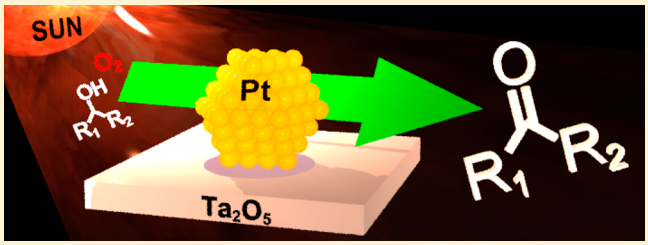

INTRODUCTION

Aerobic oxidation by heterogeneous catalysts with O_2 as an oxidant is an essential reaction for organic synthesis from the viewpoint of green and sustainable chemistry.[1] Photocatalytic oxidation with O_2 has also been studied extensively with semiconductor TiO_2,[2−6] because it oxidizes several types of substrates such as alcohols, amines, hydrocarbons, and sulfides at room temperature. One critical issue for practical application of the photocatalytic processes is the low catalytic activity under irradiation of visible light (λ >400 nm), the main component of solar irradiance. Several TiO_2 materials doped with nitrogen,[7,8] sulfur,[9,10] carbon,[11,12] or boron atoms[13,14] have been proposed to extend the absorption edge into the visible region. All of these doped catalysts, however, suffer from low quantum yields for the reaction (<0.5%), because they inherently contain a large number of crystalline lattices that behave as charge recombination centers.[15] The creation of visible-light-driven photocatalysts that efficiently promote aerobic oxidation is still a challenge.

A metal particles/semiconductor system, driven by an absorption of visible light by metal particles,[16] is one of the promising photocatalysts for aerobic oxidation. As shown in Scheme 1, Au[17−24] or Pt particles[25−28] supported on semiconductors such as TiO_2, CeO_2, ZrO_2, and $SrTiO_3$ absorb visible light and produce *hot electrons* (e_{hot}^-) via an intra- or interband transition of 6sp or 5d band electrons.[29−31] These e_{hot}^- are injected into the semiconductor conduction band (CB) through the metal/semiconductor interface. The positive charges (*hot holes*, δ^+) formed on the metal oxidize substrates, while the CB electrons (e_{CB}^-) are consumed by the reduction of O_2, promoting aerobic oxidation even at room temperature. The quantum yields for the reactions are, however, <5% (at 550 nm), although much higher than those obtained by the doped catalysts (<0.5%).[7−14] The rate-determining step is the injection of e_{hot}^- into the semiconductor CB because it requires the energy to overcome the Schottky barrier (ϕ_B) created at the metal/semiconductor interface.[32,33] Development of a new catalyst that promotes the reaction without e_{hot}^- injection is therefore a key to efficient aerobic oxidation.

Recently, some metal absorption systems that promote reactions on the metal particles "without e_{hot}^- injection" have been proposed.[34] Laser photoexcitation ($\lambda \geq$450 nm) of Au particles (ca. 10−20 nm) supported on SiO_2 promotes H_2 dissociation ($H_2 + D_2 \rightarrow 2HD$) at room temperature by the e_{hot}^- photoformed on the Au particles.[35] In that, a TiO_2

Received: April 20, 2015
Published: July 9, 2015

ACS Publications © 2015 American Chemical Society

DOI: 10.1021/jacs.5b04062
J. Am. Chem. Soc. 2015, 137, 9324−9332

Scheme 1. Aerobic Oxidation on a Metal/Semiconductor System under Irradiation of Visible Light[a]

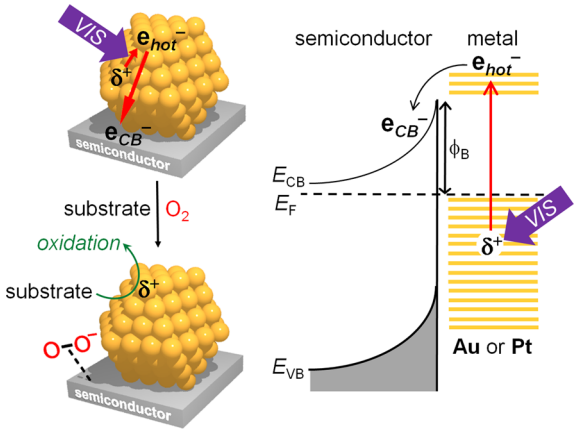

[a] E_F and ϕ_B [= $W - \chi$ (eV)] are the Fermi level and the height of Schottky barrier, respectively [W = work function of metal (eV); χ = electron affinity of semiconductor CB (eV)].

support is less effective because the e_{hot}^- injection into the TiO_2 CB decreases the number of e_{hot}^- on the Au particles.[36] Aerobic oxidation of carbon monoxide (CO) is promoted on Pt particles (ca. 2−3 nm) supported on α-Al_2O_3 under visible light irradiation by a Xe lamp with relatively high quantum yield (ca. 5% at 550 nm).[37] The reaction is promoted by photoexcitation of CO molecules adsorbed on the Pt surface. In that, a high temperature (>373 K) is necessary for high catalytic activity. Aerobic oxidation of ethylene ($C_2H_4 + {}^1/_2O_2 \rightarrow C_2H_4O$) is promoted on Ag nanocubes (75 nm edge length) supported on α-Al_2O_3 by visible light irradiation with a Xe lamp.[38,39] It is considered that, based on ab initio calculation by density functional theory (DFT), the reaction occurs via a donation of e_{hot}^- to O_2 adsorbed on the Ag surface. The formed anionic oxygen species are proposed to be the active species for oxidation, although the species are not detected directly. The Ag/α-Al_2O_3 system promotes the reaction with very high quantum yield (ca. 60% at 380−800 nm) but needs high reaction temperature (>373 K). This is probably because vibrational activation (dissociation) of the active oxygen species by thermal stimuli is required for oxidation.[40] The design of a visible-light-driven metal particle system that promotes aerobic oxidation at room temperature is therefore still a challenge.

Herein, we report that visible-light-induced aerobic oxidation at room temperature is facilitated by Pt nanoparticles (~5 nm diameter) supported on semiconductor Ta_2O_5. These Pt nanoparticles possess very high electron density due to the strong Pt−Ta_2O_5 interaction. This enhances interband transition of the Pt 5d electrons by absorbing visible light. A large number of e_{hot}^- produced on the photoactivated Pt surface directly activate O_2 and create active peroxide species for oxidation. The formation of the species was detected by spectroscopic analysis. The Pt/Ta_2O_5 catalysts successfully promote aerobic oxidation of alcohols with significantly high quantum yield, ~25% (at 550 nm).

RESULTS AND DISCUSSION

Catalyst Preparation. The Pt_2/Ta_2O_5 catalyst loaded with 2 wt % Pt (= Pt/Ta_2O_5 × 100) was prepared by impregnation of $H_2PtCl_6{\cdot}6H_2O$ onto Ta_2O_5 (average particle size, 1.3 μm; BET surface area, 2.6 $m^2\ g^{-1}$) followed by H_2 reduction at 673 K.[41,42] Transmission electron microscopy (TEM) observation of the catalyst (Figure 1a and 1b) exhibits spherical Pt particles

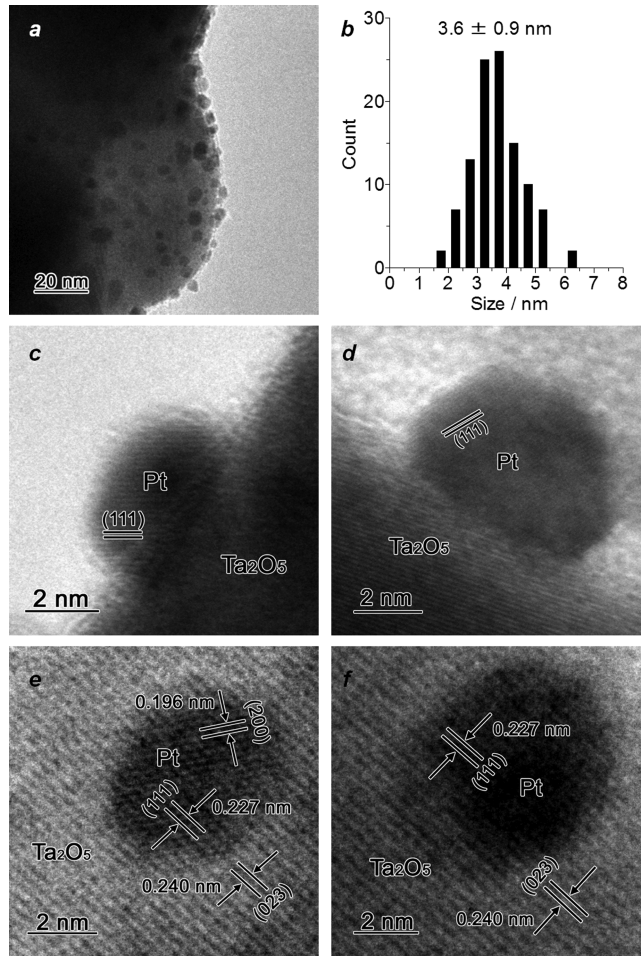

Figure 1. (a) Typical TEM image of Pt_2/Ta_2O_5 catalyst and (b) size distribution of the Pt particles. (c−f) High-resolution TEM images of the catalyst.

with an average diameter 3.6 nm. High-resolution TEM images (Figure 1c and 1d) reveal that these particles can be indexed as *fcc* structures, as is the case for bulk Pt (JCPDS 04-0802). As shown in Figure 2a, diffuse-reflectance (DR) UV−vis spectra reveal that bare Ta_2O_5 absorbs light at λ <330 nm, whereas Pt_2/Ta_2O_5 shows a broad absorption band at λ >350 nm, assigned to interband transition of 5d electrons on the Pt particles.[43] These data clearly suggest that visible light activates the Pt particles but does not activate the Ta_2O_5 support.

Catalytic Activity. High catalytic activity of Pt_2/Ta_2O_5 is demonstrated by aerobic oxidation of 2-propanol (2-PrOH). The reactions were performed by stirring the catalyst (10 mg) in 2-PrOH (5 mL) under an O_2 balloon (~1 atm) in the dark or under visible light irradiation with a Xe lamp (λ >450 nm). The temperature of the solution was kept rigorously at 298 ± 0.5 K by a digitally controlled water bath. Figure 3 summarizes the amount of acetone formed by 6 h reaction in the dark (black) or under photoirradiation (white). It is noted that all of the systems selectively produce acetone (mass balance >99%), as is the case for related metal/semiconductor systems.[17−28] Bare Ta_2O_5 is inactive for the reaction in both conditions. In contrast, Pt_2/Ta_2O_5 produces acetone relatively efficiently even in the dark (ca. 0.3 mmol). The striking aspect of this catalyst is

DOI: 10.1021/jacs.5b04062
J. Am. Chem. Soc. 2015, 137, 9324−9332

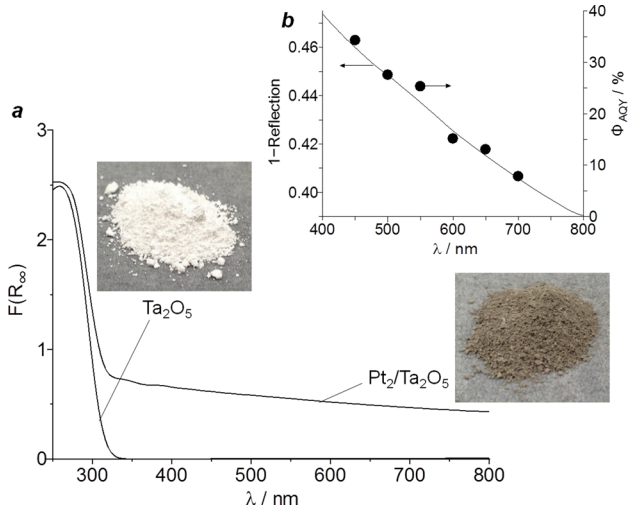

Figure 2. (a) DR UV−vis spectra of the catalysts and (b) action spectrum for aerobic oxidation of 2-PrOH on Pt_2/Ta_2O_5. The apparent quantum yield for acetone formation (Φ_{AQY}) was calculated with the equation: Φ_{AQY} (%) = [{($Y_{VIS} - Y_{dark}$) × 2}/(photon number entered into the reaction vessel)] × 100, where Y_{VIS} and Y_{dark} are the amounts of acetone formed under visible light irradiation (λ >450 nm) and in the dark conditions, respectively.

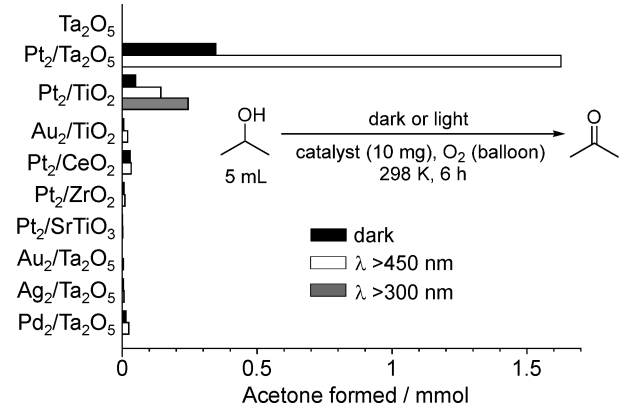

Figure 3. Amount of acetone formed by aerobic oxidation of 2-PrOH on the respective catalysts at 298 K, (black) in the dark, (white) under visible light irradiation (λ >450 nm; light intensity at 450−800 nm is 16.8 mW cm^{-2}), and (gray) under UV−visible light irradiation (λ >300 nm; light intensity at 300−800 nm is 21.0 mW cm^{-2}). DR UV−vis spectra of the catalysts are summarized in Figure S2 (Supporting Information), and spectral irradiances for the light sources are shown in Figure S3 (Supporting Information).

the drastic activity enhancement by visible light irradiation; about 5 times the amount of acetone (ca. 1.6 mmol) is produced by the irradiation of λ >450 nm light. Other semiconductors (TiO_2, CeO_2, ZrO_2, and $SrTiO_3$) loaded with Pt or Au particles, which promote the reaction by the e_{hot}^- injection mechanism,[17−28] exhibit only a minor activity enhancement (<0.2 mmol) even by visible light irradiation. In addition, Au, Ag, or Pd particles supported on Ta_2O_5 show almost no activity enhancement. These data suggest that Pt particles, when supported on Ta_2O_5, specifically promote efficient aerobic oxidation under visible light irradiation.

It is generally accepted that a Pt/TiO_2 catalyst shows very high photocatalytic activity under UV irradiation because Pt particles efficiently trap the CB electrons on the photoexcited TiO_2 and create a charge separated state.[44−46] However, as shown by the gray bar in Figure 3, a Pt_2/TiO_2 catalyst, when irradiated by UV−visible region light (λ >300 nm), produces only a small amount of acetone (ca. 0.25 mmol). This emphasizes extraordinary high catalytic activity of Pt_2/Ta_2O_5 under visible light irradiation. It must be noted that, as shown in Figure S1 (Supporting Information), Pt_2/Ta_2O_5 maintains its activity even after prolonged photoirradiation (~36 h), indicating that the catalyst is stable under photoirradiation.

Figure 2b shows the action spectrum for aerobic oxidation of 2-PrOH on Pt_2/Ta_2O_5 obtained by monochromatic light irradiation. A good correlation is observed between the absorption spectrum of the catalyst and the apparent quantum yields for acetone formation (Φ_{AQY}). This suggests that interband transition of 5d electrons on the Pt particles by absorbing visible light indeed promotes the reaction. It is noted that the Φ_{AQY} obtained by 550 nm light irradiation is ~25%, which is much higher than that for early reported metal nanoparticle/semiconductor systems (<5%)[17−28] and doped catalysts (<0.5%).[7−14]

No e_{hot}^- Injection from Pt to Ta_2O_5. On Pt_2/Ta_2O_5, the e_{hot}^- produced on the photoactivated Pt particles are not injected into the Ta_2O_5 CB. The work function of the Pt particles (average diameter: 3.6 nm) is determined to be W = 6.0 eV,[47−49] and the electron affinity of Ta_2O_5 CB is χ = 3.2 eV.[50,51] The height of Schottky barrier created at the Pt−Ta_2O_5 interface is therefore calculated with the equation, $\phi_B = W - \chi$,[32,33] to be 2.8 eV (λ = 443 nm). This is larger than the energy of light irradiated in the present photoreaction system (λ >450 nm). This suggests that, on Pt/Ta_2O_5, the high ϕ_B suppresses the e_{hot}^- injection from Pt particles to Ta_2O_5 CB. The no e_{hot}^- injection is confirmed by electron spin resonance (ESR) analysis of the catalysts. The Pt_2/TiO_2 catalyst, which promotes aerobic oxidation by the e_{hot}^- injection mechanism,[25−28] was irradiated by visible light (λ >450 nm) with O_2 at 298 K. As shown by the blue line in Figure 4a, the sample, when subjected to ESR analysis at 77 K, shows strong signals assigned to superoxide anion formed on the TiO_2 surface (g_{xx} = 2.002, g_{yy} = 2.009, g_{zz} = 2.028).[52] This suggests that, as shown in Scheme 1, the e_{hot}^- photoformed on the Pt particles are indeed injected

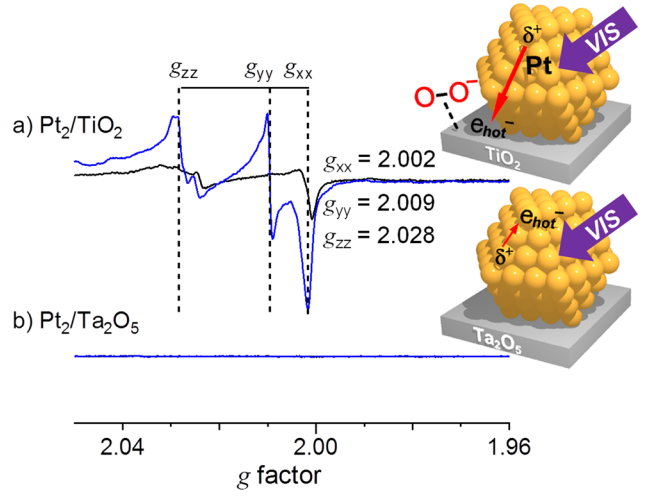

Figure 4. ESR spectra of (a) Pt_2/TiO_2 and (b) Pt_2/Ta_2O_5 measured with O_2 at 77 K. The catalysts were left at 298 K with 20 Torr of O_2 (black) in the dark or (blue) under visible light irradiation (λ >450 nm) for 3 h. After evacuation, the respective samples were subjected to analysis at 77 K.

DOI: 10.1021/jacs.5b04062
J. Am. Chem. Soc. 2015, 137, 9324−9332

into the TiO_2 CB and reduce O_2 on the TiO_2 surface. In contrast, as shown by the blue line in Figure 4b, visible light irradiation of Pt_2/Ta_2O_5 with O_2 does not create superoxide signal. This clearly indicates that e_{hot}^- injection from Pt particles to Ta_2O_5 does not occur.

Catalysis Mechanism on Pt/Ta_2O_5. Mechanism for aerobic oxidation on Pt/Ta_2O_5 can be explained by Scheme 2. In the dark condition, Pt particles partially donate their 5d

Scheme 2. (A) Energy Diagram and (B) Proposed Mechanism for Aerobic Oxidation on Pt/Ta_2O_5 in the Dark or under Visible Light

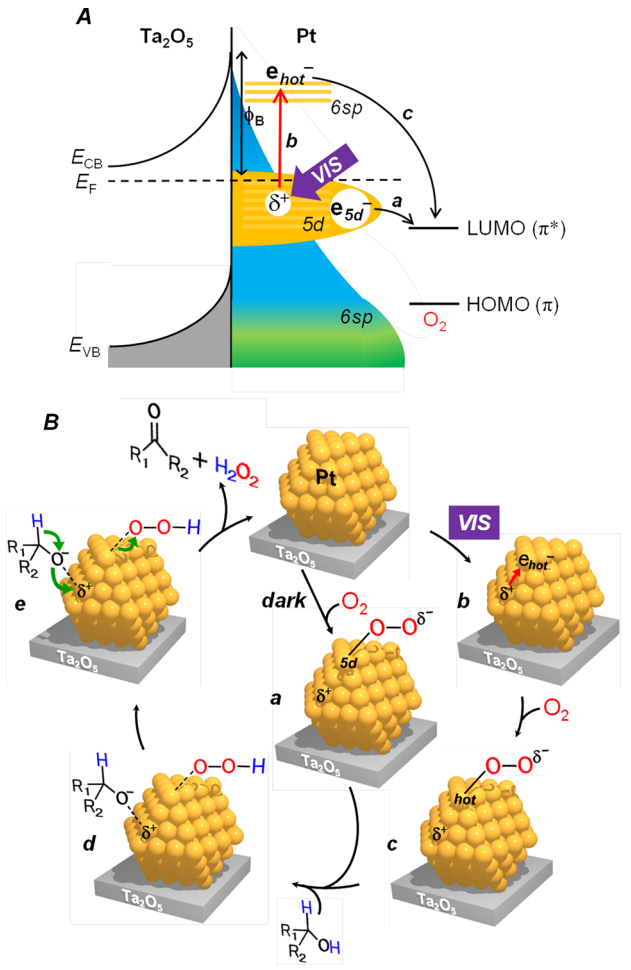

electrons (e_{5d}^-) to LUMO (π^*) of O_2 (Scheme 2A.a).[53−55] This activates O_2 and produces anionic peroxo species (Pt_{5d}–O–$O^{\delta-}$, Scheme 2B.a).[56,57] Visible light absorption of the Pt particles promotes interband transition of their e_{5d}^-, producing a large number of e_{hot}^- (Scheme 2A.b and 2B.b). The e_{hot}^- also activate O_2 by partial electron donation (Scheme 2A.c),[39] producing a large number of anionic peroxo species (Pt_{hot}–O–$O^{\delta-}$; Scheme 2B.c). These peroxo species (Pt_{5d}–O–$O^{\delta-}$ and Pt_{hot}–O–$O^{\delta-}$) behave as the active species for oxidation: they abstract the α-hydrogen of alcohos and produce alcoholate and hydroperoxide species on the Pt surface (Scheme 2B.d).[58] Subsequent abstraction of β-hydrogen from the alcoholate species produces the corresponding carbonyl product (Scheme 2B.e).

Formation of Peroxo Species. In the present Pt/Ta_2O_5 system, anionic peroxo species (Pt_{hot}–O–$O^{\delta-}$) formed by e_{hot}^- donation to O_2 on the Pt surface act as the active species. As reported,[39] aerobic oxidation of ethylene on the Ag/α-Al_2O_3 catalyst under visible light irradiation is also considered to occur via e_{hot}^- donation to O_2 on the Ag surface. Similar anionic peroxo species (Ag–O–$O^{\delta-}$) are proposed to act as active species based on the DFT calculation. The formation of the Pt_{hot}–O–$O^{\delta-}$ species (Scheme 2B.c) on the Pt surface by visible light irradiation is confirmed by the diffuse-reflectance infrared Fourier transform (DRIFT) analysis of O_2 adsorbed onto the catalysts. As shown in Figure 5a, bare Ta_2O_5 measured

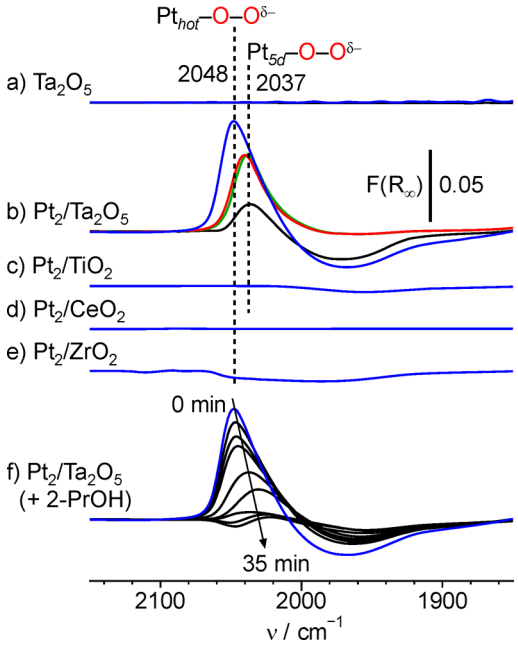

Figure 5. (a–e) DRIFT spectra of O_2 adsorbed onto the catalysts, measured (black) in the dark at 303 K, (green) in the dark at 343 K, (blue) under 450 nm light irradiation at 303 K, or (red) under 450 nm light irradiation at 343 K. The catalyst (20 mg) was evacuated (6.8×10^{-3} Torr) at 423 K for 3 h. O_2 (1.5 Torr) was introduced to the cell at the designated temperature and left for 1 h in the dark or under photoirradiation. (f) Time-dependent spectral change (intervals: 5 min) monitored in the dark at 303 K after addition of 2-PrOH (7.5×10^{-1} Torr) to the Pt_2/Ta_2O_5 sample obtained after 450 nm light irradiation at 303 K with O_2 for 1 h (sample b, blue).

with O_2 shows almost no signal in the dark (black) or under irradiation of 450 nm light (blue). In contrast, as shown in Figure 5b (black), Pt_2/Ta_2O_5 measured with O_2 in the dark creates a band at 2037 cm^{-1}, assigned to O–O vibration of peroxo species.[59] This suggests that, as shown in Scheme 2A.a and 2B.a, the peroxo species (Pt_{5d}–O–$O^{\delta-}$) are indeed produced by partial e_{5d}^- donation to O_2.[56,57] In contrast, visible light irradiation of Pt_2/Ta_2O_5 with O_2 (Figure 5b, blue) creates a very strong O–O band at the blue-shifted position (2048 cm^{-1}). This suggests that, as shown in Scheme 2A.c and 2B.c, a large number of more anionic peroxo species (Pt_{hot}–O–$O^{\delta-}$) are indeed produced via a strong e_{hot}^- donation to O_2. It is noted that, as shown in Figure 5b (green), the Pt_2/Ta_2O_5 catalyst, when treated with O_2 at high temperature (343 K) in the dark, shows a red-shifted signal at 2037 cm^{-1}, which is similar to that obtained in the dark at 303 K (black). This indicates that, under present photoirradiation conditions, photothermal conversion[60] on the Pt particles does not occur.[61−64] This again suggests that, as shown in Scheme

DOI: 10.1021/jacs.5b04062
J. Am. Chem. Soc. 2015, 137, 9324−9332

2A.c and 2B.c, visible light irradiation of the Pt/Ta_2O_5 catalyst produces peroxo species ($Pt_{hot}-O-O^{\delta-}$) via an e_{hot}^- donation to O_2.

In contrast, as shown in Figure 5c–e, Pt_2/TiO_2, Pt_2/CeO_2, and Pt_2/ZrO_2 do not show O–O band even under visible light irradiation. The O–O band intensities on the respective catalysts are consistent with the activity data (Figure 3). This suggests that, on Pt/Ta_2O_5, the enhanced e_{hot}^- formation on the Pt particles efficiently activates O_2 and produces a large number of peroxo species; this is the crucial factor for high catalytic activity. Figure 5f shows the time-dependent change in the $Pt_{hot}-O-O^{\delta-}$ signal on the Pt_2/Ta_2O_5 catalyst, when left in the dark at 303 K after addition of 2-PrOH in the gas phase. The signal decreases with time, and GC analysis of the fouling on the resulting catalyst detected a formation of acetone. These findings clearly suggest that abstraction of alcohol hydrogen by the peroxo species (Scheme 2B.c → d) indeed promotes aerobic oxidation.

Electron Density of Pt Particles on Ta_2O_5. The efficient e_{hot}^- formation on the Pt particles, when supported on Ta_2O_5, is due to the high electron density of the Pt particles by strong $Pt-Ta_2O_5$ interaction. The Fermi levels of Pt and Ta_2O_5 lie at −5.65 eV (bulk)[49] and −4.25 eV,[65] respectively (from vacuum level), indicating that there is a large Fermi level difference between Pt and Ta_2O_5. Strong metal–support interaction,[66−68] if it occurs, may therefore promote electron donation from Ta_2O_5 to Pt for the Fermi level balancing and result in high electron density of Pt particles. X-ray photoelectron spectroscopy (XPS) of the catalysts confirms this. As shown in Figure S4 (Supporting Information), the Pt/Ta_2O_5 catalyst exhibits Pt 4f 5/2 and 7/2 peaks at 73.0 and 69.7 eV, respectively. In contrast, the Pt peaks for other catalysts (Pt/TiO_2, Pt/CeO_2, and Pt/ZrO_2) appear at higher binding energy. This indicates that the Pt particles on Ta_2O_5 are indeed charged more negatively. These data clearly indicate that strong $Pt-Ta_2O_5$ interaction enhances electron donation from Ta_2O_5 to Pt at the interface and, hence, increases electron density of the Pt particles.[69]

It is well-known that a reducible metal oxide support is crucial for strong metal–support interaction, where the oxygen vacancies of the support adjacent to the reduced metal cations facilitate strong adhesion of metal.[30] A correlation between the reducibility of supports and the interaction strength with metal indicates strong metal–Ta_2O_5 interaction.[70] Strong $Pt-Ta_2O_5$ interaction is supported by HRTEM observations. As shown in Figure 2e,f, the Pt(111) plane is adsorbed onto the Ta_2O_5(023) plane. Their lattice spacings are determined to be 0.227 and 0.240 nm, respectively. A good agreement of the spacings (deviation: ∼6%) indicates epitaxial growth of Pt particles on the Ta_2O_5(023) plane.[71,72] These data suggest that strong adhesion of Pt onto the oxygen vacancies of Ta_2O_5 surface facilitates strong $Pt-Ta_2O_5$ interaction.

The high electron density of the Pt particles on Ta_2O_5 is further confirmed by DRIFT analysis of carbon monoxide (CO) adsorbed onto the Pt particles, because the stretching frequency of the adsorbed CO depends strongly on the electron density of metal particles.[57,73] Figure 6 shows the DRIFT spectra of CO adsorbed onto the catalysts at 303 K. Bare Ta_2O_5 measured in the dark (Figure 6a) shows almost no signal, indicating that its surface is inactive for CO adsorption. As shown in Figure 6b (black), Pt_2/Ta_2O_5 shows a CO stretching band at 2046 cm^{-1}. Other Pt-loaded catalysts show blue-shifted bands (Figure 6c–e). This indicates that the Pt

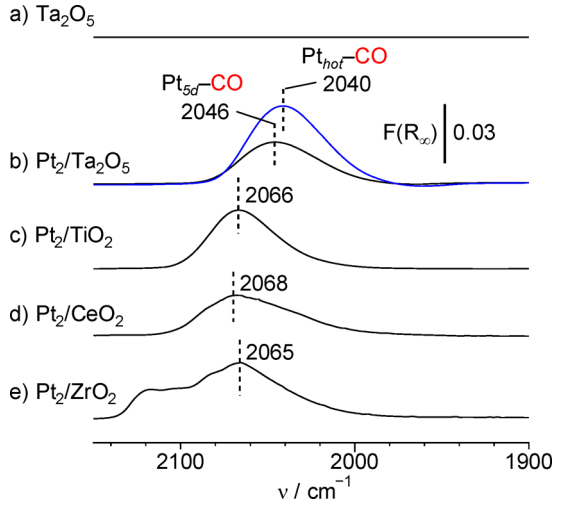

Figure 6. DRIFT spectra of CO adsorbed onto the catalysts (black) in the dark or (blue) under 450 nm light irradiation at 303 K. The catalysts (20 mg) were evacuated (6.8×10^{-3} Torr) at 423 K for 3 h. CO (1.5 Torr) was introduced into the cell at 303 K and left for 1 h in the dark or under photoirradiation.

particles on Ta_2O_5 indeed possess high electron density. The XPS and DRIFT data therefore imply that the high electron density of the Pt particles on Ta_2O_5 enhances interband transition of e_{5d}^- and produces a large number of e_{hot}^-.

As shown in Figure 6b (blue), CO molecules, when adsorbed onto Pt_2/Ta_2O_5 under 450 nm light irradiation, exhibit a red-shifted and stronger stretching at 2040 cm^{-1}. This indicates that the Pt particles are charged more negatively by visible light irradiation. This is because CO molecules are strongly adsorbed onto the Pt surface via stronger electron donation from the photoformed e_{hot}^-. This is consistent with the DRIFT data for the formation of peroxo species (Figure 5b, blue). The results strongly support the proposed mechanism for efficient aerobic oxidation via O_2 activation by the photogenerated e_{hot}^- (Scheme 2).

Effect of Pt Amount. The catalytic activity of the e_{hot}^--induced aerobic oxidation on Pt/Ta_2O_5 depends on the amount of Pt loaded. The Pt_x/Ta_2O_5 catalysts with different Pt loadings [x (wt %) = $Pt/Ta_2O_5 \times 100$; x = 0.5–3 wt %] were prepared by H_2 reduction at 673 K. As shown in Figure 7a (orange), these catalysts contain Pt particles with similar sizes (3.6–3.8 nm). The black and white bars show the amounts of acetone formed by aerobic oxidation of 2-PrOH on the catalysts for 6 h in the dark or under irradiation of visible light, respectively. The activity enhancement by photoirradiation increases with the Pt loadings because an increased number of surface Pt atoms produces a larger number of e_{hot}^-. Among the catalysts, Pt_2/Ta_2O_5 shows the largest activity enhancement, and further Pt loadings (x > 2.5) are ineffective. This is because, as often observed for related metal/semiconductor systems,[74] larger Pt loadings lead to an inefficient electron donation from Ta_2O_5 to Pt and creates Pt particles with lower electron density. This is confirmed by higher binding energy for the Pt XPS peaks of Pt_3/Ta_2O_5 than that of Pt_2/Ta_2O_5 (Figure S4, Supporting Information). As a result of this, the Pt_2/Ta_2O_5 catalyst containing Pt particles with high electron density enhances interband transition of their e_{5d}^- and exhibits the highest activity enhancement by visible light irradiation.

DOI: 10.1021/jacs.5b04062
J. Am. Chem. Soc. 2015, 137, 9324–9332

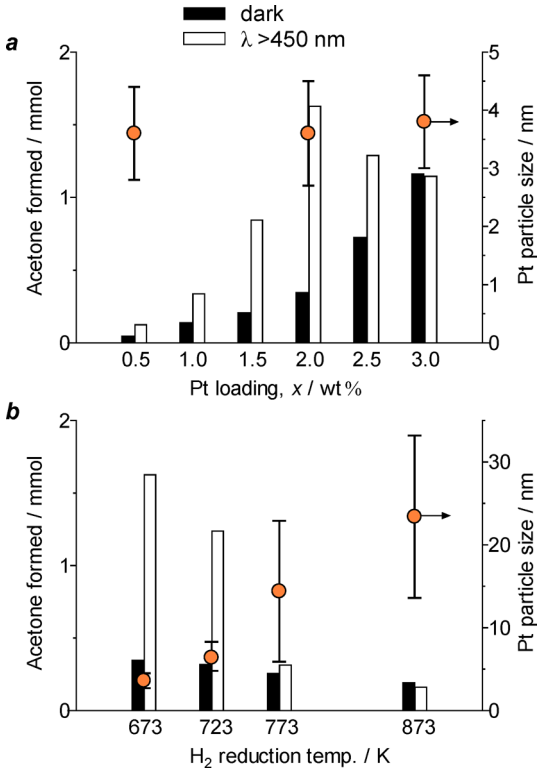

Figure 7. Effect of (a) Pt loading (x) of Pt_x/Ta_2O_5 catalysts and (b) H_2 reduction temperature of Pt_2/Ta_2O_5 catalysts on the amount of acetone formed by aerobic oxidation of 2-PrOH (6 h reaction), performed (black) in the dark or (white) under visible light irradiation at 298 K. The reaction conditions are identical to those in Figure 3. Circles denote the average diameters of Pt particles on the respective catalysts. The H_2 reduction temperature for the catalysts (a) is 673 K, and the Pt loading of the catalysts (b) is 2 wt %, respectively. Typical TEM images of the catalysts and size distributions of the Pt particles are summarized in Figure S5 (Supporting Information).

Effect of Pt Particle Size. The size of Pt particles also affects the catalytic activity. The Pt_2/Ta_2O_5 catalysts were prepared by H_2 reduction at different temperatures (673–873 K) while maintaining 2 wt % Pt loading. As shown in Figure 7b (orange), the size of Pt particles increases with a rise in reduction temperature due to the sintering of Pt particles.[26] It is noted that, as shown in Figure S6 (Supporting Information), X-ray diffraction (XRD) patterns of the catalysts reveal that phase transition of Ta_2O_5 support scarcely occurs during H_2 reduction at this temperature range. As shown by the bar data in Figure 7b, the increase in the Pt particle size significantly decreases the activity enhancement by visible light irradiation. The size increase decreases the number of surface Pt atoms. This may decrease the number of e_{hot}^-, probably resulting in decreased activity enhancement. These data indicate that the Pt/Ta_2O_5 catalyst with 2 wt % Pt, containing <5 nm Pt particles, efficiently promotes interband transition of their e_{5d}^- and exhibits the largest activity enhancement by visible light irradiation.

Effect of Reaction Temperature. The catalytic activity of Pt_2/Ta_2O_5 is also affected by reaction temperature. Figure 8 summarizes the results of aerobic oxidation at different reaction temperatures on the Pt_2/Ta_2O_5 catalyst prepared by H_2 reduction at 673 K. The dark activity (black bars) increases with a rise in reaction temperature because this enhances the e_{5d}^- donation to O_2[53−55] and produces a larger number of

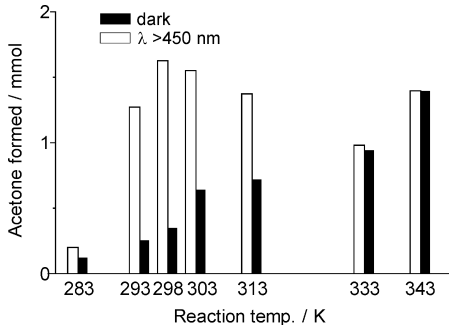

Figure 8. Effect of reaction temperature on the amount of acetone formed during oxidation of 2-PrOH (6 h reaction) with Pt_2/Ta_2O_5 catalyst, performed (black) in the dark or (white) under visible light irradiation. The reaction conditions are identical to those in Figure 3.

active peroxo species (Pt_{5d}–O–$O^{\delta-}$), as shown in Scheme 2A and 2B.a. In contrast, under visible light irradiation (white bars), the highest activity is obtained at 298 K, and the activity decreases at lower or higher temperature. Two factors may affect the reaction. The activity decrease at <298 K is probably due to the decrease in electron conductivity of Pt particles with decreasing temperature.[75−77] This may suppress the e_{hot}^- formation on the Pt surface and, hence, decrease the catalytic activity.

In contrast, the activity decrease at higher temperature is probably due to the enhanced e_{5d}^- donation to O_2. This may suppress interband transition of e_{5d}^- and results in decreased e_{hot}^- formation. As shown in Figure 8, a rise in temperature at >298 K decreases the photocatalytic activity while increasing the dark activity, and almost no photocatalytic reaction occurs at >333 K. This means that acceleration of the dark reaction at higher temperature suppresses photocatalytic reaction. This is confirmed by DRIFT analysis. As shown by the black line (Figure 5b), Pt_2/Ta_2O_5 measured with O_2 at 303 K in the dark shows a peak at 2037 cm^{-1}, assigned to the Pt_{5d}–O–$O^{\delta-}$ species formed via an e_{5d}^- donation to O_2. As shown by the green line, the sample, when measured at 343 K in the dark, shows a stronger peak at the same position, indicating that e_{5d}^- donation to O_2 is accelerated by thermal activation of e_{5d}^- at higher temperature. In contrast, as shown by the blue line, the sample measured at 303 K under visible light irradiation shows a peak at 2048 cm^{-1}, assigned to the Pt_{hot}–O–$O^{\delta-}$ species formed via an e_{hot}^- donation to O_2. However, as shown by the red line, the sample measured at 343 K under visible light irradiation shows a red-shifted peak at 2037 cm^{-1}, which is similar to that measured at 343 K in the dark (green). These data suggest that the e_{hot}^- formation is suppressed at higher temperature. Thermal activation of e_{5d}^- at higher temperature enhances the e_{5d}^- donation to O_2. This may suppress the interband transition of e_{5d}^- and results in decreased e_{hot}^- formation.

The above findings suggest that visible light irradiation at around room temperature is the condition suitable for maximizing the activity of the Pt_2/Ta_2O_5 catalyst for aerobic oxidation. It must be noted that, at this photoirradiation condition, the Pt_2/Ta_2O_5 catalyst selectively oxidizes various types of alcohols. As summarized in Table S1 (Supporting Information), reactions of aliphatic (linear and cyclic) and benzylic alcohols on Pt_2/Ta_2O_5 successfully produce the corresponding aldehydes and ketones with very high yields

DOI: 10.1021/jacs.5b04062
J. Am. Chem. Soc. 2015, 137, 9324–9332

(>90%), even in the presence of electron-withdrawing Cl and NO_2 substituents.

CONCLUSION

We found that Pt nanoparticles (~5 nm diameter), when supported on Ta_2O_5, behave as visible-light-driven catalysts for efficient aerobic oxidation at room temperature. Visible light absorption of the Pt particles produces a large number of e_{hot}^- via the enhanced interband transition of their 5d electrons. They activate O_2 and produce a large number of peroxide species behaving as key active species for oxidation. The basic concept presented here, based on the enhanced e_{hot}^- formation on the metal particles by an appropriate semiconductor support and the promotion of photocatalysis without e_{hot}^- injection into the semiconductor CB, may contribute to the creation of more active catalyst driven by visible light and to the design of sunlight-driven organic synthesis.

EXPERIMENTAL SECTION

General. All of the reagents used were supplied from Wako, Tokyo Kasei, and Sigma-Aldrich and used without further purification. Water was purified by the Milli Q system. Ta_2O_5 and $SrTiO_3$ were purchased from Wako. TiO_2 (JRC-TIO-1 and JRC-TIO-4), ZrO_2 (JRC-ZRO-3), and CeO_2 (JRC-CEO-3) were kindly supplied from the Catalyst Society of Japan (Japan Reference Catalyst). These properties are summarized in Table S2 (Supporting Information).

Catalyst Preparation. Pt_x/Ta_2O_5 [x (wt %) = $Pt/Ta_2O_5 \times 100$; x = 0.5, 1, 1.5, 2, 2.5, or 3] were prepared as follows: Ta_2O_5 (1 g) was added to water (40 mL) containing $H_2PtCl_6{\cdot}6H_2O$ (13.3, 26.8, 40.4, 54.2, 68.1, or 82.1 mg). The solvents were removed by evaporation at 353 K with vigorous stirring for 12 h. The obtained powders were dried under air flow and reduced under H_2 flow at the identical temperature. Unless otherwise noted, the H_2 reduction was carried out at 673 K. The heating rate was 2 K min^{-1}, and the holding time at the designated temperature was 2 h, respectively. Pt_2/TiO_2 (JRC-TIO-1), Pt/CeO_2, Pt_2/ZrO_2, and $Pt_2/SrTiO_3$ were prepared in a similar manner to that of Pt_2/Ta_2O_5. Ag_2/Ta_2O_5 and Pd_2/Ta_2O_5 were also prepared in a similar manner, with $AgNO_3$ (32 mg) or $Pd(NO_3)_2$ (44 mg) as a metal source.

Au_2/Ta_2O_5 and Au_2/TiO_2 were prepared by a deposition–precipitation method.[19] Ta_2O_5 or TiO_2 (JRC-TIO-4, 1 g) was added to water (50 mL) containing $HAuCl_4{\cdot}4H_2O$ (46 mg). The pH of the solution was adjusted to ~7 with 1 mM NaOH, and the solution was stirred at 353 K for 3 h. The particles were recovered by centrifugation, washed thoroughly with water, and dried at 353 K for 12 h. The powders were calcined under air flow, where the heating rate was 2 K min^{-1} and the holding time at 673 K was 2 h, respectively.

Photoreaction. Catalyst (10 mg) was added to 2-PrOH (5 mL) within a Pyrex glass tube (φ 12 mm; capacity, 20 mL). The tube was sealed with a rubber septum cap. The catalyst was dispersed well by ultrasonication for 5 min, and O_2 was bubbled through the solution for 5 min. The tube with an O_2 balloon was immersed in a temperature-controlled water bath, and the temperatures of the solutions were kept rigorously at the designated temperature (deviation: ±0.5 K).[19] The tube was photoirradiated with magnetic stirring using a 2 kW Xe lamp (USHIO Inc., λ >300 nm). The light intensity at 300–800 nm was 21.0 mW cm^{-2}. A glass filter (CS3-72; Kopp Glass Inc.) was used to give light wavelength at λ >450 nm, where the light intensity at 450–800 nm was 16.8 mW cm^{-2}. After photoreaction, the catalyst was recovered by centrifugation, and the resulting solution was analyzed by GC-FID (Shimadzu, GC-1700).

Action Spectrum Analysis. Catalyst (8 mg) was suspended in 2-PrOH (2 mL) within a Pyrex glass tube (φ 12 mm; capacity, 20 mL). The tube was sealed with a rubber septum cap. The catalyst was dispersed well by ultrasonication for 5 min, and O_2 was bubbled through the solution for 5 min. The tube with an O_2 balloon was photoirradiated with magnetic stirring by a 2 kW Xe lamp (USHIO Inc.), where the incident light was monochromated by band-pass glass filters (Asahi Techno Glass Co.).[23] The full-width at half-maximum (fwhm) of the lights was 11–16 nm. The temperature of the solutions during photoirradiation was kept at 298 ± 0.5 K in a temperature-controlled water bath. The photon number entered into the reaction vessel was determined with a spectroradiometer (USR-40; USHIO Inc.).

ESR Measurement. ESR spectra were recorded at the X-band using a Bruker EMX-10/12 spectrometer with a 100 kHz magnetic field modulation at a microwave power level of 10.0 mW, where microwave power saturation of the signal does not occur.[27] The magnetic field was calibrated with 1,1′-diphenyl-2-picrylhydrazyl (DPPH). Catalyst (10 mg) was placed in a quartz ESR tube and evacuated at 423 K for 3 h. After cooling the tube to room temperature, O_2 (20 Torr) was introduced to the tube and left for 3 h at 298 K in the dark or under photoirradiation using a Xe lamp (2 kW; USHIO Inc.) at λ >450 nm (with CS3-72; Kopp Glass Inc.). The ESR tube was then evacuated for 10 min to remove the excess amount of O_2 and subjected to analysis at 77 K.

DRIFT Analysis. The spectra were measured on a FT/IR-610 system (JASCP Corp.),[78] equipped with an in situ DR cell (Heat Chamber HC-500, ST Japan, Inc.). The catalyst (20 mg) was placed in the DR cell, and the cell was evacuated (6.8×10^{-3} Torr) at 423 K for 3 h. O_2 or CO (1.5 Torr) was introduced to the cell at the designated temperature. The cell was left at the temperature for 3 h in the dark or under irradiation of 450 nm monochromatic light with a Xe lamp (300 W; Asahi Spectra Co. Ltd.; Max-302) equipped with 450 nm band-pass filter. The fwhm of the light was 10 nm, and the light intensity was 68 μW cm^{-2}, respectively. The cell was then evacuated for 10 min to remove the excess amount of O_2 or CO and subjected to analysis at 303 K.

Other Analysis. TEM observations were performed on a FEI Tecnai G2 20ST analytical electron microscope operated at 200 kV.[79] XRD patterns were measured on a Philips X'Pert-MPD spectrometer. XPS measurements were performed using a JEOL JPS9000MX spectrometer with Mg Kα radiation as the energy source. C 1s binding energy at 284.8 eV was used as a reference for the calibration of XPS lines.[80] Diffuse-reflectance UV–vis spectra were measured on an UV–vis spectrometer (Jasco Corp.; V-550 with Integrated Sphere Apparatus ISV-469) with $BaSO_4$ as a reference.

ASSOCIATED CONTENT

Supporting Information

Time-profiles for the acetone formation (Figure S1), DR UV–vis spectra of catalysts (Figure S2), spectral irradiance for light sources (Figure S3), XPS charts for catalysts (Figure S4), TEM images of catalysts and size distribution of Pt particles (Figure S5), XRD patterns of catalysts (Figure S6), results for photoreaction of various alcohols (Table S1), and properties of semiconductors used (Table S2). The Supporting Information is available free of charge on the ACS Publications website at DOI: 10.1021/jacs.5b04062.

AUTHOR INFORMATION

Corresponding Author

*shiraish@cheng.es.osaka-u.ac.jp

Notes

The authors declare no competing financial interest.

ACKNOWLEDGMENTS

This work was supported by the Grant-in-Aid for Scientific Research (no. 26289296) from the Ministry of Education, Culture, Sports, Science and Technology, Japan (MEXT), and by the Precursory Research for Embryonic Science and Technology (PRESTO) from Japan Science and Technology Agency (JST).

DOI: 10.1021/jacs.5b04062
J. Am. Chem. Soc. 2015, 137, 9324–9332

REFERENCES

(1) Sheldon, R. A.; Arends, I. W. C. E.; Dijksman, A. *Catal. Today* **2000**, *57*, 157−166.
(2) Fox, M. A.; Dulay, M. T. *Chem. Rev.* **1993**, *93*, 341−357.
(3) Maldotti, A.; Molinari, A.; Amadelli, R. *Chem. Rev.* **2002**, *102*, 3811−3836.
(4) Palmisano, G.; Augugliaro, V.; Pagliaro, M.; Palmisano, L. *Chem. Commun.* **2007**, 3425−3437.
(5) Fagnoni, M.; Dondi, D.; Ravelli, D.; Albini, A. *Chem. Rev.* **2007**, *107*, 2725−2756.
(6) Shiraishi, Y.; Hirai, T. *J. Photochem. Photobiol., C* **2008**, *9*, 157−170.
(7) Asahi, R.; Morikawa, T.; Ohwaki, T.; Aoki, K.; Taga, Y. *Science* **2001**, *293*, 269−271.
(8) Miyauchi, M.; Ikezawa, A.; Tobimatsu, H.; Irie, H.; Hashimoto, K. *Phys. Chem. Chem. Phys.* **2004**, *6*, 865−870.
(9) Ohno, T.; Akiyoshi, M.; Umebayashi, T.; Asai, K.; Mitsui, T.; Matsumura, M. *Appl. Catal., A* **2004**, *265*, 115−121.
(10) Yan, X.; Ohno, T.; Nishijima, K.; Abe, R.; Ohtani, B. *Chem. Phys. Lett.* **2006**, *429*, 606−610.
(11) Sakthivel, S.; Kisch, H. *Angew. Chem., Int. Ed.* **2003**, *42*, 4908−4911.
(12) Irie, H.; Watanabe, Y.; Hashimoto, K. *Chem. Lett.* **2003**, *32*, 772−773.
(13) Zhao, W.; Ma, W.; Chen, C.; Zhao, J.; Shuai, Z. *J. Am. Chem. Soc.* **2004**, *126*, 4782−4783.
(14) Zaleska, A.; Sobczak, J. W.; Grabowska, E.; Hupka, J. *Appl. Catal., B* **2008**, *78*, 92−100.
(15) Chen, X.; Mao, S. S. *Chem. Rev.* **2007**, *107*, 2891−2959.
(16) Primo, A.; Corma, A.; García, H. *Phys. Chem. Chem. Phys.* **2011**, *13*, 886−910.
(17) Tian, Y.; Tatsuma, T. *J. Am. Chem. Soc.* **2005**, *127*, 7632−7637.
(18) Kowalska, E.; Mahaney, O. O. P.; Abe, R.; Ohtani, B. *Phys. Chem. Chem. Phys.* **2010**, *12*, 2344−2355.
(19) Tsukamoto, D.; Shiraishi, Y.; Sugano, Y.; Ichikawa, S.; Tanaka, S.; Hirai, T. *J. Am. Chem. Soc.* **2012**, *134*, 6309−6315.
(20) Tanaka, A.; Hashimoto, K.; Kominami, H. *J. Am. Chem. Soc.* **2012**, *134*, 14526−14533.
(21) Kimura, K.; Naya, S.; Jin-nouchi, Y.; Tada, H. *J. Phys. Chem. C* **2012**, *116*, 7111−7117.
(22) Naya, S.; Kimura, K.; Tada, H. *ACS Catal.* **2013**, *3*, 10−13.
(23) Sugano, Y.; Shiraishi, Y.; Tsukamoto, D.; Ichikawa, S.; Tanaka, S.; Hirai, T. *Angew. Chem., Int. Ed.* **2013**, *52*, 5295−5299.
(24) Liu, L.; Li, P.; Adisak, B.; Ouyang, S.; Umezawa, N.; Ye, J.; Kodiyath, R.; Tanabe, T.; Ramesh, G. V.; Ueda, S.; Abe, H. *J. Mater. Chem. A* **2014**, *2*, 9875−9882.
(25) Zai, W.; Xue, S.; Zhu, A.; Luo, Y.; Tian, Y. *ChemCatChem* **2011**, *3*, 127−130.
(26) Shiraishi, Y.; Tsukamoto, D.; Sugano, Y.; Shiro, A.; Ichikawa, S.; Tanaka, S.; Hirai, T. *ACS Catal.* **2012**, *2*, 1984−1992.
(27) Shiraishi, Y.; Sakamoto, H.; Sugano, Y.; Ichikawa, S.; Hirai, T. *ACS Nano* **2013**, *7*, 9287−9297.
(28) Shiraishi, Y.; Sakamoto, H.; Fujiwara, K.; Ichikawa, S.; Hirai, T. *ACS Catal.* **2014**, *4*, 2418−2425.
(29) Hao, Q.; Juluri, B. K.; Zheng, Y. B.; Wang, B.; Chiang, I.-K.; Jensen, L.; Crespi, V.; Eklund, P. C.; Huang, T. J. *J. Phys. Chem. C* **2010**, *114*, 18059−18066.
(30) Park, J. Y.; Baker, L. R.; Somorjai, G. A. *Chem. Rev.* **2015**, *115*, 2781−2817.
(31) Link, S.; El-Sayed, M. A. *Int. Rev. Phys. Chem.* **2000**, *19*, 409−453.
(32) Schottky, W. *Eur. Phys. J. A* **1939**, *113*, 367−414.
(33) Nakato, Y.; Ueda, K.; Yano, H.; Tsubomura, H. *J. Phys. Chem.* **1988**, *92*, 2316−2324.
(34) Brongersma, M. L.; Halas, N. J.; Nordlander, P. *Nat. Nanotechnol.* **2015**, *10*, 25−34.
(35) Mukherjee, S.; Zhou, L.; Goodman, A. M.; Large, N.; Ayala-Orozco, C.; Zhang, Y.; Nordlander, P.; Halas, N. J. *J. Am. Chem. Soc.* **2014**, *136*, 64−67.
(36) Mukherjee, S.; Libisch, F.; Large, N.; Neumann, O.; Brown, L. V.; Cheng, J.; Lassiter, J. B.; Carter, E. A.; Nordlander, P.; Halas, N. J. *Nano Lett.* **2013**, *13*, 240−247.
(37) Kale, M. J.; Avanesian, T.; Xin, H.; Yan, J.; Christopher, P. *Nano Lett.* **2014**, *14*, 5405−5412.
(38) Christopher, P.; Xin, H.; Linic, S. *Nat. Chem.* **2011**, *3*, 467−472.
(39) Christopher, P.; Xin, H.; Marimuthu, A.; Linic, S. *Nat. Mater.* **2012**, *11*, 1044−1050.
(40) Avanesian, T.; Christopher, P. *J. Phys. Chem. C* **2014**, *118*, 28017−28031.
(41) Shiraishi, Y.; Ikeda, M.; Tsukamoto, D.; Tanaka, S.; Hirai, T. *Chem. Commun.* **2011**, *47*, 4811−4813.
(42) Shiraishi, Y.; Takeda, Y.; Sugano, Y.; Ichikawa, S.; Tanaka, S.; Hirai, T. *Chem. Commun.* **2011**, *47*, 7863−7865.
(43) Bigall, N. C.; Härtling, T.; Klose, M.; Simon, P.; Eng, L. M.; Eychmüller, A. *Nano Lett.* **2008**, *8*, 4588−4592.
(44) Szabó-Bárdos, E.; Czili, H.; Horváth, A. *J. Photochem. Photobiol., A* **2003**, *154*, 195−201.
(45) Subramanian, V.; Wolf, E. E.; Kamat, P. V. *J. Am. Chem. Soc.* **2004**, *126*, 4943−4950.
(46) Zhang, H.; Chen, G.; Bahnemann, D. W. *J. Mater. Chem.* **2009**, *19*, 5089−5121.
(47) The work function of metal particles (W) depends on their sizes and is defined as the following equation: $W = W_{bulk} + 1.08/d$ (ref 48). The work function of bulk Pt (W_{bulk}) is 5.7 eV (ref 49). The W of Pt particles (average diameter: d = 3.6 nm) on the Pt_2/Ta_2O_5 catalyst is therefore determined to be 6.0 eV.
(48) Wood, D. M. *Phys. Rev. Lett.* **1981**, *46*, 749−749.
(49) Bardeen, J. *Phys. Rev.* **1947**, *71*, 717−727.
(50) Yamamoto, T. A.; Nakagawa, T.; Seino, S.; Nitani, H. *Appl. Catal., A* **2010**, *387*, 195−202.
(51) Liang, D.; Gao, J.; Wang, J.; Chen, P.; Wei, Y.; Hou, Z. *Catal. Commun.* **2011**, *12*, 1059−1062.
(52) Anpo, M.; Che, M.; Fubini, B.; Garrone, E.; Giamello, E.; Paganini, M. C. *Top. Catal.* **1999**, *8*, 189−198.
(53) Li, T.; Balbuena, P. B. *J. Phys. Chem. B* **2001**, *105*, 9943−9952.
(54) Tominaga, H.; Nagai, M. *Electrochim. Acta* **2009**, *54*, 6732−6739.
(55) Liu, K.; Lei, Y.; Wang, G. *J. Chem. Phys.* **2013**, *139*, 204306.
(56) Kim, Y. D.; Fischer, M.; Ganteför, G. *Chem. Phys. Lett.* **2003**, *377*, 170−176.
(57) Tsunoyama, H.; Ichikuni, N.; Sakurai, H.; Tsukuda, T. *J. Am. Chem. Soc.* **2009**, *131*, 7086−7093.
(58) Ishida, T.; Nagaoka, M.; Akita, T.; Haruta, M. *Chem. - Eur. J.* **2008**, *14*, 8456−8460.
(59) Li, C.; Domen, K.; Maruya, K.; Onishi, T. *J. Am. Chem. Soc.* **1989**, *111*, 7683−7687.
(60) Chen, X.; Zhu, H.-Y.; Zhao, J.-C.; Zheng, Z.-F.; Gao, X.-P. *Angew. Chem., Int. Ed.* **2008**, *47*, 5353−5356.
(61) Photothermal conversion on the photoirradiated Pt particles scarcely occurs in the present system. The temperature increase on the surface of an individual Pt particle in solution under photoirradiation can roughly be estimated by the equation, $\Delta T = \sigma_{abs} I/(4\pi R_{eq}\beta\kappa)$, where σ_{abs} = absorption cross section, I = intensity of the incident light, R_{eq} = radius of a sphere with the same volume as the particle, β = thermal capacitance coefficient dependent on the nanoparticle aspect ratio, κ = thermal conductivity of solvent (ref 62). The σ_{abs} value for <100 nm Pt particle is reported to be $<1 \times 10^{-14}$ m^2 (ref 63). Other parameters for our catalysts are as follows: R_{eq} <25 nm, I = 168 W m^{-2}, β = 1, κ = 0.137 W m^{-1} K^{-1} (ref 64). The theoretical temperature increase, ΔT, is determined with these parameters to be 3.9×10^{-5} K. This very small temperature increase suggests that photothermal conversion scarcely occurs in the present Pt/Ta_2O_5 system.
(62) Baffou, G.; Quidant, R.; García de Abajo, F. J. *ACS Nano* **2010**, *4*, 709−716.
(63) Langhammer, C.; Kasemo, B.; Zorić, I. *J. Chem. Phys.* **2007**, *126*, 194702.
(64) Li, C. C. *AIChE J.* **1976**, *22*, 927−930.

DOI: 10.1021/jacs.5b04062
J. Am. Chem. Soc. 2015, 137, 9324−9332

(65) Chun, W.-J.; Ishikawa, A.; Fujisawa, H.; Takata, T.; Kondo, J. N.; Hara, M.; Kawai, M.; Matsumoto, Y.; Domen, K. *J. Phys. Chem. B* **2003**, *107*, 1798−1803.
(66) Horsley, J. A. *J. Am. Chem. Soc.* **1979**, *101*, 2870−2874.
(67) Sexton, B. A.; Hughes, A. E.; Foger, K. *J. Catal.* **1982**, *77*, 85−93.
(68) Shiraishi, Y.; Kofuji, Y.; Kanazawa, S.; Sakamoto, H.; Ichikawa, S.; Tanaka, S.; Hirai, T. *Chem. Commun.* **2014**, *50*, 15255−15258.
(69) The Pt 4f peaks on the Pt_2/Ta_2O_5 catalyst scarcely change even after visible light irradiation (Figure S4, Supporting Information). This clearly indicates that oxidation states and electron density of Pt particles do not change after photoreaction.
(70) Tauster, S. J.; Fung, S. C.; Baker, R. T. K.; Horsley, J. A. *Science* **1981**, *211*, 1121−1125.
(71) Bernal, S.; Botana, F. J.; Calvino, J. J.; López, C.; Pérez-Omil, J. A.; Rodríguez-Izquierdo, J. M. *J. Chem. Soc., Faraday Trans.* **1996**, *92*, 2799−2809.
(72) Ketteler, G.; Ranke, W. *Phys. Rev. B: Condens. Matter Mater. Phys.* **2002**, *66*, 033405.
(73) Yoon, B.; Häkkinen, H.; Landman, U.; Wörz, A. S.; Antonietti, J.−M.; Abbet, S.; Judai, K.; Heiz, U. *Science* **2005**, *307*, 403−407.
(74) Uchihara, T.; Matsumura, M.; Yamamoto, A.; Tsubomura, H. *J. Phys. Chem.* **1989**, *93*, 5870−5874.
(75) Hamanaka, Y.; Nakamura, A.; Omi, S.; Del Fatti, N.; Vallée, F.; Flytzanis, C. *Appl. Phys. Lett.* **1999**, *75*, 1712−1714.
(76) Yeshchenko, O. A.; Bondarchuk, I. S.; Alexeenko, A. A.; Kotko, A. V. *Funct. Mater.* **2013**, *20*, 357−365.
(77) Yeshchenko, O. A.; Bondarchuk, I. S.; Gurin, V. S.; Dmitruk, I. M.; Kotko, A. V. *Surf. Sci.* **2013**, *608*, 275−281.
(78) Shiraishi, Y.; Hirakawa, H.; Togawa, Y.; Hirai, T. *ACS Catal.* **2014**, *4*, 1642−1649.
(79) Shiraishi, Y.; Tanaka, K.; Shirakawa, E.; Sugano, Y.; Ichikawa, S.; Tanaka, S.; Hirai, T. *Angew. Chem., Int. Ed.* **2013**, *52*, 8304−8308.
(80) Shiraishi, Y.; Kanazawa, S.; Kofuji, Y.; Sakamoto, H.; Ichikawa, S.; Tanaka, S.; Hirai, T. *Angew. Chem., Int. Ed.* **2014**, *53*, 13454−13459.

DOI: 10.1021/jacs.5b04062
J. Am. Chem. Soc. 2015, 137, 9324−9332